

AD\_\_\_\_\_

Award Number: W81XWH-10-1-084G

TITLE: InVivo Imaging of Myelination for Drug Discovery and Development in Multiple Sclerosis

PRINCIPAL INVESTIGATOR: Yanming Wang, Ph.D.

CONTRACTING ORGANIZATION: Case Western Reserve University  
Cleveland, OH 44106-1714

REPORT DATE: October 2012

TYPE OF REPORT: Annual

PREPARED FOR: U.S. Army Medical Research and Materiel Command  
Fort Detrick, Maryland 21702-5012

DISTRIBUTION STATEMENT: Approved for Public Release;  
Distribution Unlimited

The views, opinions and/or findings contained in this report are those of the author(s) and should not be construed as an official Department of the Army position, policy or decision unless so designated by other documentation.

REPORT DOCUMENTATION PAGE				Form Approved OMB No. 0704-0188	
Public reporting burden for this collection of information is estimated to average 1 hour per response, including the time for reviewing instructions, searching existing data sources, gathering and maintaining the data needed, and completing and reviewing this collection of information. Send comments regarding this burden estimate or any other aspect of this collection of information, including suggestions for reducing this burden to Department of Defense, Washington Headquarters Services, Directorate for Information Operations and Reports (0704-0188), 1215 Jefferson Davis Highway, Suite 1204, Arlington, VA 22202-4302. Respondents should be aware that notwithstanding any other provision of law, no person shall be subject to any penalty for failing to comply with a collection of information if it does not display a currently valid OMB control number. PLEASE DO NOT RETURN YOUR FORM TO THE ABOVE ADDRESS.					
1. REPORT DATE October 2012		2. REPORT TYPE Annual		3. DATES COVERED 30 September 2011 – 29 September 2012	
4. TITLE AND SUBTITLE  InVivo Imaging of Myelination for Drug Discovery and Development in Multiple Sclerosis				5a. CONTRACT NUMBER	
				5b. GRANT NUMBER W81XWH-10-1-0842	
				5c. PROGRAM ELEMENT NUMBER	
6. AUTHOR(S)  Yanming Wang, Ph.D.  E-Mail: yxw91@case.edu				5d. PROJECT NUMBER	
				5e. TASK NUMBER	
				5f. WORK UNIT NUMBER	
7. PERFORMING ORGANIZATION NAME(S) AND ADDRESS(ES)  Case Western Reserve University Cleveland, OH 44106-1714				8. PERFORMING ORGANIZATION REPORT NUMBER	
9. SPONSORING / MONITORING AGENCY NAME(S) AND ADDRESS(ES) U.S. Army Medical Research and Materiel Command Fort Detrick, Maryland 21702-5012				10. SPONSOR/MONITOR'S ACRONYM(S)	
				11. SPONSOR/MONITOR'S REPORT NUMBER(S)	
12. DISTRIBUTION / AVAILABILITY STATEMENT Approved for Public Release; Distribution Unlimited					
13. SUPPLEMENTARY NOTES					
14. ABSTRACT  During the first funding cycle, we have worked closely with Dr. Miller to develop a series of animal models to assess the efficacy of the imaging compounds that he has developed to detect demyelination and remyelination in the intact brain and spinal cord. We have also begun to test the ability of the imaging probes to assay remyelination in response to potential therapeutic treatments. The key research accomplishments are highlighted below:  1. Design, synthesis and evaluation of coumarin-based molecular probes for imaging of myelination. (Wang et al, J. Med. Chem. 2011) 2. Longitudinal imaging of myelination using a near infra-red probe. (Wang et al, J. Neuroscience 2011) 3. Longitudinal [11C]CIC-PET Imaging in the spinal cord of a rat model of focal demyelination.					
15. SUBJECT TERMS Positron emission tomography, imaging, myelination, molecular probes, multiple sclerosis.					
16. SECURITY CLASSIFICATION OF:			17. LIMITATION OF ABSTRACT	18. NUMBER OF PAGES	19a. NAME OF RESPONSIBLE PERSON
a. REPORT	b. ABSTRACT	c. THIS PAGE			USAMRMC
U	U	U	UU	35	19b. TELEPHONE NUMBER (include area code)

## Table of Contents

	<u>Page</u>
Introduction.....	2
Body.....	3
Reportable Outcomes.....	4
Conclusion.....	30
References.....	31

## INTRODUCTION

Multiple Sclerosis (MS) is the most commonly acquired autoimmune disease, currently affecting over 400,000 people in the US, and 2 million people worldwide. MS is characteristic of demyelination in the central nervous system (CNS), a process largely associated with the breakdown and loss of myelin sheaths. As a result, the efficient conduction of axonal impulses is hampered, leading to various neurological disabilities and cognitive impairment. In the healthy CNS, demyelinated axons can be reinvested with new myelin sheaths through a highly effective regenerative process. The remyelination process involves the recruitment of oligodendrocyte precursor cells, which are subsequently activated and distributed to the damaged axons. However, the remyelination process is often disrupted in MS. This leads to incomplete myelin repair, and subsequent irreversible axonal damage.

*In vivo* imaging of demyelination and remyelination in the CNS, especially changes in the spinal cord is of particular importance as much of the physical disability and cognitive impairment in MS are associated with myelin damage (Bot et al., 2004; Ciccarelli et al., 2007). For this reason, our laboratory has been developing myelin-specific radiotracers for *in vivo* PET imaging of myelination. Over the past decade, we have identified several lead compounds that readily enter the brain and selectively localize in the myelinated white matter (Stankoff et al., 2006; Wu et al., 2006; Wu et al., 2008; Wang et al., 2009; Wang et al., 2010b; Wang et al., 2010a; Wu et al., 2010; Wang et al., 2011). In our previous studies, one of the lead compounds (MeDAS) has been radiolabeled with positron-emitting carbon-11, and used for PET imaging of myelination (Wu et al., 2008; Wu et al., 2010). We demonstrated that [ $^{11}\text{C}$ ]MeDAS can readily penetrate the blood-brain barrier (BBB) and localize in various brain regions in proportion to the extent of myelination. [ $^{11}\text{C}$ ]MeDAS-PET can be used to quantitatively detect myelin changes in the brain in mouse models with myelin pathology (Wu et al., 2010).

Encouraged by the results, we evaluated the potential of [ $^{11}\text{C}$ ]MeDAS-PET as a sensitive and specific imaging marker to detect demyelination and remyelination in the spinal cord, which would be a very powerful tool for screening novel therapies aimed at myelin repair. In this work, we report *in vivo* characterization of [ $^{11}\text{C}$ ]MeDAS-PET in the spinal cord in different animal models such as lysolethicin (lysophosphatidyl choline, LPC) induced rat model of focal demyelination, and experimental autoimmune encephalomyelitis (EAE) rat models. Subsequently, we conducted the first image-guided myelin repair therapy based on hepatocyte growth factor (HGF), which has been identified as a key component in mesenchymal stem cells (MSCs) that mediates remyelination. We demonstrated that [ $^{11}\text{C}$ ]MeDAS-PET can be used to quantitatively determine the dose response and to optimize the extent of remyelination in the spinal cord.

## **Body**

With a Synergistic Idea Award from the Department of Defense, we plan to further optimize the newly developed myelin-imaging techniques and use them to evaluate the efficacy of novel therapeutic agents in different animal models of MS. These studies will allow us to identify the best candidate(s) that are uniquely suited for future clinical trials. *We hypothesize that myelin repair can be achieved by therapeutic agents that are aimed at promotion of remyelination. Further, we specifically hypothesize that the efficacy of remyelinating agents can be quantified in vivo at various levels of myelination such that the regional distribution and concentration of probes will be consistent with the myelin neuropathology present.* Our approach will be to further develop myelin-imaging agents that can longitudinal monitor myelin changes in different animal models of demyelination. Next, we will use PET imaging to evaluate the *in vivo* myelin

repair properties of therapeutic agents. We will then validate the *in vivo* studies by correlation with postmortem histology studies. Completion of this project will allow us to identify the lead candidate for Phase I clinical trial that can be initiated immediately following completion of this project.

In the first year of this project, we have reached all the milestones listed in Specific Aim 1. In the second year, we report our progress on the tasks listed in Specific Aim 2.

## **MATERIAL AND METHODS**

Animal surgery and care was performed in accordance with the Institutional Animal Care and Use Committee of Case Western Reserve University.

### **Induction of focal demyelination in the spinal cord**

In this model, LPC was directly injected into the spinal cord of Sprague-Dawley (SD) female rats (8-10 weeks old, 220-240 g) as reported (Kerstetter et al., 2009). Animals were anesthetized using a mixture of rodent cocktail. For post-operative pain relief, Torbugesic (2 mg/kg) was subcutaneously administered prior to surgical procedure. A T10 laminectomy was performed by first making lateral longitudinal incisions in the paraspinal muscles from the middle of T-11 through the middle of T-12. A beveled microcapillary glass needle attached through small diameter tubing to a microinjection system (using a 10 µl Hamilton syringe) was then directed 1 mm into the dorsal column of the spinal cord with the aid of a Stoelting stereotaxic manipulator. LPC was injected into the dorsal column in a dose of 1.5 µl at 1% concentration, at a rate 0.25 µl/min. It was then necessary to wait 2-3 additional minutes prior to dose administration before removing the needle, to ensure there was no backflow of the solution. The animals were then allowed to recover in a clean cage sitting on a heating pad.

### **Induction of EAE in rats**

Two sets of 8-week old female rats, 3 Lewis and 3 SD, were acquired from Charles River Laboratories, in Wilmington MA. They were kept in our animal facility for one week after arrival, before immunization. Recombinant myelin oligodendrocyte glycoprotein (rMOG 1-125, from Biogen Idec.) inoculum was freshly prepared by initially diluting the rMOG in 0.01M phosphate buffered saline (PBS, pH 7.4) to a final concentration of 2 mg/ml. Then, equal volumes of MOG/PBS and Complete Freund's Adjuvant were mixed thoroughly (CFA (2mg/ml), Chondrex, Inc, WA). The emulsion was gently centrifuged, and loaded slowly into a 1-ml syringe for subcutaneous injection. Rats were anesthetized with rodent cocktail before emulsion injections, and administered 100 µl of inoculum by intradermal injection at the base of the tail. Each rat received 50 µg of rMOG 1-125.

After MOG induction, animals were weighed and scored daily for signs of EAE according to the following scale: 0, no disease; 1, tail paralysis; 2, hind limb weakness; 3, hind limb paralysis; 4, hind limb paralysis and forelimb weakness; 5, moribund or dead.

### **Induction of rat lipopolysaccharide (LPS) neuroinflammation model**

Female SD rats (n=3, 6-8 weeks of age) were anesthetized with rodent cocktail and positioned in a stereotaxic frame (Stoelting). The scalp was incised and retracted so the cortex and corpus callosum could be targeted using the following stereotaxic coordinates: (relative to bregma) anterior–posterior (AP), 3.0 mm; medial–lateral (ML), 1.0mm; and dorsal–ventral (DV), 2.0 mm for cortex, and AP, 0.0 mm; ML, 2.0mm; and DV, 4.5 mm for corpus callosum. Two small holes

were drilled in the skull, and a 33S gauge needle attached to a 10  $\mu$ L Hamilton Syringe was lowered into the cortex and corpus callosum via the prior coordinates. A mini injector pump (Stoelting) controlled the infusion of 3  $\mu$ L of LPS (E.coli, serotype 055:B5, 1mg/ml) at a rate of 0.25  $\mu$ L/min, after which the needle was left in place for 2 min to prevent liquid reflux out of the brain parenchyma. The incision was then closed, and the animals were allowed to recover on a heating pad.

## **Histopathology**

After microPET studies, histopathological studies were conducted. The animals were killed by a transcardial perfusion of saline followed by 4% polyformaldehyde (PFA) under anesthesia. The spinal cord and brain were carefully removed and postfixed in 4% PFA overnight, followed by 10%, 20% and 30% sucrose solution. They were then sectioned at 20 $\mu$ m on a cryostat, and mounted directly onto Superfrost Plus microscope slides. The slides were then subject to either neuroinflammation staining or myelin staining using Black gold, Luxol Fast Blue, or MeDAS staining as previously described (Mi et al., 2007; Wu et al., 2008; Wang et al., 2009).

## **Neuroinflammation staining**

After the perfused tissue was cryoprotected in sucrose and frozen in OCT, 20 $\mu$ M serial sections were made on a Microm HM525. They were air-dried and kept at -20°C until staining. The samples were brought to room temperature and allowed to air-dry again, followed by rehydration in PBS. The PBS was removed, and the sections were blocked with 5-10% Normal Goat Serum in 0.1% Triton-X 100 in PBS for one hour at room temperature. The antibodies, IBA1 (Rabbit polyclonal, Wako Cat. #019-19741) or GFAP (Rabbit polyclonal, Dako Z0334), were diluted 1:500 in block, and the sections were incubated overnight at 4°C. The next day,



the sections were rinsed, incubated 1.5 hours in the secondary antibody (Invitrogen goat anti-Rabbit IgG Alexa-594), then rinsed again and mounted in Vectashield. The sections were imaged on a Leica DM 5500B microscope, using a Leica DFC 500 camera.

### ***Ex vivo* fluorescent tissue staining of myelin**

A dose of (25 mg/kg) of MeDAS was administered via tail-vein injection to a Female SD rat. At 2 hours post-injection, the rat was deeply anesthetized and perfused transcardially with saline and 4% paraformaldehyde (PFA). The brain and spinal cord were removed and postfixed by immersion in 4% PFA overnight, then dehydrated in 30% sucrose solution and embedded in a freezing compound (OCT, Fisher Scientific, Suwanee, GA). They were cryostat sectioned at 20  $\mu$ m on a microtome, and mounted on superfrost slides (Fisher Scientific) with fluoromount-G mounting media (Vector Laboratories, Burlingame, CA). Due to the fact that MeDAS is inherently fluorescent, MeDAS staining of myelin was able to be directly examined under a Leica DRMB microscope equipped for fluorescence.

### **HFG treatment**

In these studies an LPC lesion was induced as described above, and the animals were then treated with 2 doses of HGF systemically. Because there is an initial immunological response to the demyelinating lesion, delivery of the first dose was delayed for 4 days after lesion induction. Animals were randomly assigned to either control (saline, n=6) or experimental (HGF treatment, n=8) groups. The experimental group received 0.4 and 0.8  $\mu$ g/Kg of HGF via tail vein injection on days 4, 6, and 12 prior to lesion development. The controls received an equivalent volume of saline, and the animals were imaged on days 7, 14, and 21 post LPC treatment.

### **MicroPET/CT imaging of spinal cord and data acquisition**

PET imaging of [ $^{11}\text{C}$ ]MeDAS was performed using a Siemens Inveon microPET/CT scanner in the Case Center for Imaging Research. For better anatomic localization, CT co-registration was applied. For LPC treated rats, PET/CT scans were performed on days 0, 7, 14, and 21, following LPC injections in spinal cord. For EAE rats, PET scans were performed on day 0, and the first, second, and third disease episodes after MOG induction. The rats were fasted overnight prior to imaging, but had access to water. Their diet was then replenished after imaging. Before PET imaging, CT scout view was taken to ensure most of the vertebrae, especially the ilium, were placed in the co-scan field of view (FOV) where the highest image resolution and sensitivity is achieved. Approximately 37 MBq of [ $^{11}\text{C}$ ]MeDAS was injected through the tail vein, and dynamic microPET data acquisition was performed in a list mode immediately. During the scans, body temperature of the anesthetized rats was maintained at  $34\pm 2^\circ\text{C}$  with a heating lamp. Once the dynamic acquisition was done, a CT acquisition scan was performed for attenuation correction.

### **Quantitative image analysis**

Quantitative image analysis of the uptake of [ $^{11}\text{C}$ ]MeDAS in spinal cord was performed using Carimas II software. This program allows an ROI to be extrapolated from the reconstructed microPET image frames in order to determine the SUV in a specific region. Based on the PET and CT co-registered images, the rat's ilium was used as a marker to accurately identify vertebrae. For LPC treated rats, lesion vertebrae (Thoracic 11 and Thoracic12) were then defined as the regions of interest (ROI). For EAE rats, every single rat vertebrae (from Thoracic 8 to Lumbar 1) was defined as a ROI. The radioactivity data were decay-corrected and normalized by the body weight of the rats, and amount of [ $^{11}\text{C}$ ]MeDAS injected. Radioactivity concentration in the spinal cord is expressed in terms of standard uptake value (SUV)

$[(\mu\text{Ci/cc})/(\mu\text{Ci/g})]$  as a function of time. The time activity curve (TAC) for each vertebra was obtained.

### **MicroPET imaging in acute neuroinflammation rat model and data acquisition**

The rats with the brain as the desired FOV were placed in an Inveon microPET scanner under anesthesia. After a 10 min transmission scan with a Co-57 source, 37 MBq of [ $^{11}\text{C}$ ]MeDAS was administered via tail vein injection, and immediately followed by a dynamic acquisition of up to 90 min. A two-dimensional OSEM algorithm was used for image reconstruction. Decay, attenuation, and scatter correction were all performed during the image histogram and reconstruction processes. For better anatomic localization, a MRI scan was also performed. After microPET imaging, the same bed was transferred to a MRI scanner (Bruker Biospin 7.0T, Billerica, MA). The rat's head was well positioned in the center of the rat coil. A rapid-acquisition relaxation-enhanced (RARE) analysis (TR/TE = 2000/40 ms, 4 echoes, FOV = 45 mm  $\times$  45 mm, matrix = 256  $\times$  256) was used to acquire 15 contiguous 1 mm axial images of each animal's brain. Co-registration of MRI and PET images was conducted using the MATLAB-based program Compartmental Model Kinetic Analysis Tool (COMKAT). For quantitative image analysis, the whole brain was considered as a ROI, and was defined based on the co-registered images to measure the radioactivity concentration in the whole brain. The radioactivity data was decay corrected and normalized by the body weight of the rats, and amount of [ $^{11}\text{C}$ ]MeDAS injected.

### **Statistical analysis**

In this study, all data is expressed as a mean $\pm$ SD. A Student's t test was used to evaluate if there is any significant difference between each groups of studies. A  $p$  value of  $<0.05$  was accepted as significant.

## RESULTS

### *In vitro* tissue staining of the spinal cord

MeDAS is a fluorescent compound with maximum excitation and emission wavelengths of 363 and 419 nm, respectively (Wu et al., 2008). So the myelin binding property of MeDAS can be evaluated based on fluorescent microscopy. We thus conducted fluorescent tissue staining by incubating spinal cord tissue sections with a solution of MeDAS in 10% DMSO. For this purpose, a series of axial sections of the spinal cord were prepared so that both myelin-rich white matter and myelin-deficient gray matter could be visualized. We then conducted fluorescent tissue staining using spinal cords taken from wild-type, LPC-treated, and EAE rats. In addition, each MeDAS staining was correlated with Black-Gold staining, which was performed on adjacent sections. At a 10  $\mu$ M concentration, MeDAS selectively stained the spinal cord white matter. In contrast, much less staining of MeDAS was observed in the gray matter. In the wild-type spinal cord, MeDAS staining showed a fluorescent pattern that was consistent with Black-Gold staining, suggesting that MeDAS's retention is proportional to the myelin distribution throughout the spinal cord (**Figures 1 A and 1B**).

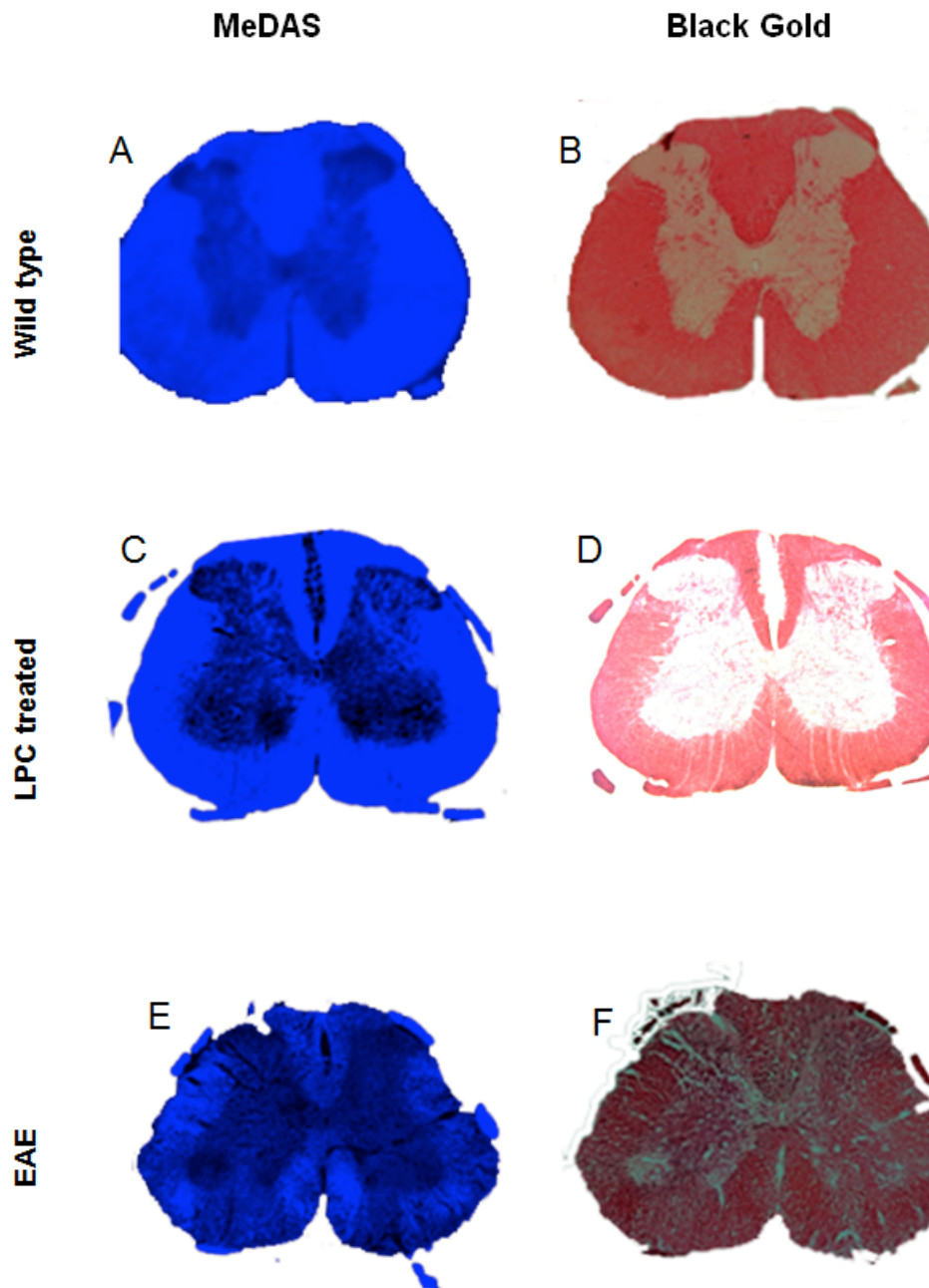


**Figure 1.** *In vitro* MeDAS staining of the spinal cord tissue sections from wild-type, LPC-treated and EAE rats that are consistent with Black-Gold staining in adjacent tissue sections.

The staining of MeDAS appears to be dependent on the presence of myelin sheaths. When myelin was damaged or lost, the fluorescent pattern was subsequently disrupted. This was

observed in fluorescent MeDAS staining of the spinal cord, with focal demyelination in the white matter that was induced by stereotactic treatment with LPC. Our previous studies have shown that LPC treatment led to focal myelin loss with significant sparing of other cell types, such as axons and astrocytes (Wang et al., 2009). As shown in **Figure 1C and 1D**, the demyelinated foci were readily visualized by MeDAS fluorescence, which was identical to Black-Gold staining in adjacent sections. Thus, MeDAS is capable of detecting demyelinated lesions. Similarly, in the spinal cord of EAE rats, MeDAS staining showed profound demyelination across the peripheral white matter in part of the most affected vertebrae, as confirmed by the Black-Gold staining (**Figure 1E and 1F**).

#### ***In situ* detection of myelin in rat brain and the spinal cord**

Following *in vitro* tissue staining, we investigated the ability of MeDAS to stain myelin tracts *in situ*. Thus, a single dose of MeDAS (20 mg/kg) was administered to wild-type SD rats via tail vein injection. Two hours later, upon perfusion, the brain and the spinal cord were then removed and sectioned, and the fluorescent MeDAS distribution was directly examined under fluorescent microscopy. As shown in **Figure 2**, the myelinated corpus callosum and the white matter of spinal cord are clearly visualized by MeDAS staining with fluorescent patterns that were consistent with Black-Gold staining in adjacent sections. These studies suggested that MeDAS readily entered the brain and spinal cord and selectively labeled the respective myelinated regions in the white matter.

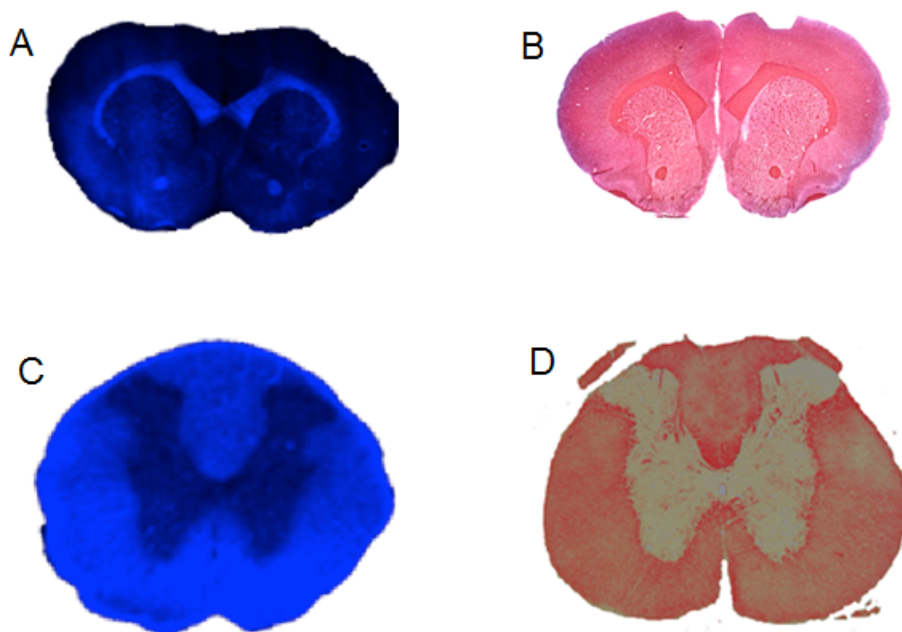


**Figure 2.** *In situ* MeDAS staining of myelin sheaths in the brain (A) and spinal cord (C) two hours after single dose (20 mg/kg) administration via tail vein injection, which correlates with Black-Gold staining in adjacent tissue sections (B and D, respectively).

### Biodistribution study

To explore the potential of MeDAS as a radiotracer for *in vivo* PET imaging, we radiolabelled MeDAS with positron emitting carbon-11 and characterized the biodistribution of [ $^{11}\text{C}$ ]MeDAS in mice at various time points. A single dose of [ $^{11}\text{C}$ ]MeDAS (3.7MBq) was administered via tail vein injection, and at 5, 15, 60, 90, and 120 minutes post-injection, radioactivity concentrations in various organs were measured. As shown in **Table 1**, at 5 min post injection, [ $^{11}\text{C}$ ]MeDAS uptake in the brain was  $6.07 \pm 3.37$  ID%/gram, suggesting that [ $^{11}\text{C}$ ]MeDAS readily penetrated the BBB and entered the brain at early time points. In the other organs examined, [ $^{11}\text{C}$ ]MeDAS showed a faster clearance at later time points except in the adrenals and bone, suggesting low non-specific binding in the body.

**Table 1.** Biodistribution of [ $^{11}\text{C}$ ]MeDAS in mice at various time points (n=3, %ID/gram).

<b>Region</b>	<b>5 min</b>	<b>15 min</b>	<b>60 min</b>	<b>90 min</b>	<b>120 min</b>
heart	3.53 $\pm$ 1.11	1.91 $\pm$ 0.17	0.67 $\pm$ 0.30	0.62 $\pm$ 0.03	0.56 $\pm$ 0.09
liver	11.56 $\pm$ 4.61	11.48 $\pm$ 0.17	1.49 $\pm$ 0.38	0.91 $\pm$ 0.11	0.62 $\pm$ 0.01
spleen	3.28 $\pm$ 0.11	3.01 $\pm$ 0.64	1.59 $\pm$ 0.75	1.35 $\pm$ 0.33	0.76 $\pm$ 0.02
lung	9.79 $\pm$ 0.51	2.75 $\pm$ 0.54	0.56 $\pm$ 0.20	0.49 $\pm$ 0.12	0.46 $\pm$ 0.02
kidney	4.98 $\pm$ 6.03	4.71 $\pm$ 0.29	0.70 $\pm$ 0.21	0.55 $\pm$ 0.09	0.34 $\pm$ 0.04
brain	6.07 $\pm$ 3.37	1.85 $\pm$ 0.38	0.31 $\pm$ 0.14	0.29 $\pm$ 0.04	0.23 $\pm$ 0.00
GI	5.80 $\pm$ 0.61	7.41 $\pm$ 1.91	1.34 $\pm$ 0.44	0.64 $\pm$ 0.10	0.54 $\pm$ 0.21
adrenals	8.06 $\pm$ 5.69	8.11 $\pm$ 6.26	5.82 $\pm$ 2.36	4.96 $\pm$ 0.31	5.77 $\pm$ 0.47
gonad	3.60 $\pm$ 1.22	7.03 $\pm$ 5.70	0.61 $\pm$ 0.30	0.43 $\pm$ 0.05	3.33 $\pm$ 0.79
bone	3.40 $\pm$ 0.83	5.01 $\pm$ 2.56	8.79 $\pm$ 7.13	5.08 $\pm$ 3.05	6.24 $\pm$ 0.06

### ***In vivo* competition studies**

To further determine the *in vivo* binding specificity of MeDAS for myelin, we conducted *in vivo* competition studies using a previously developed myelin-binding agent (BMB), as a blocking agent, which has shown high affinity for myelin (Stankoff et al., 2006). Before BMB treatment, we conducted [ $^{11}\text{C}$ ]MeDAS-PET imaging in a wild-type rat, and the radioactivity concentration in the various brain regions such as frontal cortex (FC), corpus callosum (CC), temporal lobe (TL), and cerebellum (CB) were quantified. As shown in **Figure 3A**, the uptake of [ $^{11}\text{C}$ ]MeDAS in myelin-rich regions (i.e. CC and CB) is significantly higher than that in myelin-deficient regions (TL and FC). So the specific binding of [ $^{11}\text{C}$ ]MeDAS was normalized by using the myelin-deficient TL as the reference region, where [ $^{11}\text{C}$ ]MeDAS uptake was the lowest. As shown in **Figure 3B, 3C and 3D**, the specific binding in corpus callosum, cerebellum, and frontal cortex at different time points post-injection was determined in terms of the ratio of the standardized uptake volume between the region of interest and the temporal lobe. The specific binding of CC, CB, and FC peaked at 5 min post injection, and then gradually decreased over time. When the rats were pretreated with BMB (10 mg/kg) at 3 hrs prior to [ $^{11}\text{C}$ ]MeDAS-PET imaging, the specific binding was significantly reduced. At 40 min post-injection, for example, the specific binding of CC, CB, and FC in control rats was reduced by ca. 50% in all the regions.



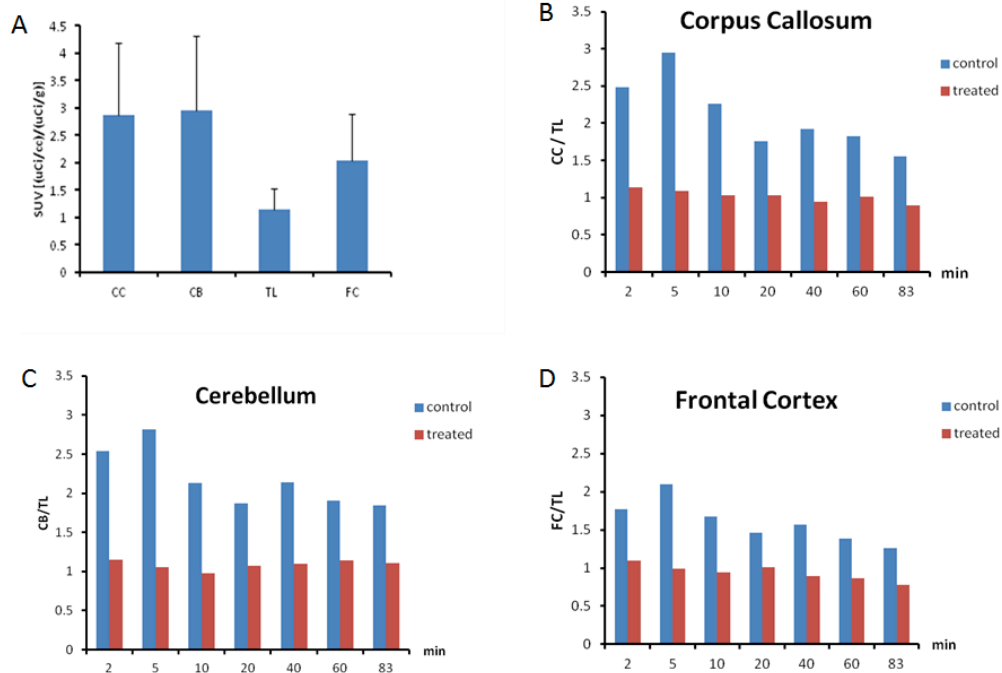


**Figure 3.** *In vivo* competition studies of [ $^{11}\text{C}$ ]MeDAS using BMB as the blocking agent. A: The average uptake of [ $^{11}\text{C}$ ]MeDAS was quantified in the white matter (i.e. corpus callosum (CC) and cerebellum (CB)) and the gray matter (i.e. temporal lobe (TL) and frontal cortex (FC)). The uptake of [ $^{11}\text{C}$ ]MeDAS was low in the myelin-deficient TL region and high in myelin-rich region (CC and CB). B, C and D: The binding of [ $^{11}\text{C}$ ]MeDAS in the CC, CB and FC in the brain were normalized using TL as the reference region and was significantly decreased after BMB treatment.

### Effects of neuroinflammation on PET imaging of demyelination

In MS pathology, both demyelination and neuroinflammation are present in the CNS. To determine if neuroinflammation has any effects on the [ $^{11}\text{C}$ ]MeDAS uptake, we prepared an acute neuroinflammation model by stereotaxic injection of LPS to the rat brain (Wenk et al., 2004). Subsequent histological analysis showed that one day after injection, profound inflammation was developed in the rat brain while myelin sheaths remained intact.

Immunohistology showed profound microglia activation and macrophages in the brain by IBA1 staining (**Figure 4A** and **4E**). A reactive form of astrocytes was also detected by GFAP staining (**Figure 4B** and **4F**). In the meantime, the myelin integrity remained intact as demonstrated by Luxol Fast Blue staining (**Figure 5C** and **5G**), and *in vitro* MeDAS staining (**Figure 4D** and **4H**). Using this neuroinflammation rat model, we conducted PET studies to determine [ $^{11}\text{C}$ ]MeDAS uptake before and after the inflammation was induced. As shown in **Figure 4I** and **4J**, [ $^{11}\text{C}$ ]MeDAS uptake was practically identical before and after LPS treatment. Thus, induction of inflammation did not alter the pharmacokinetics of [ $^{11}\text{C}$ ]MeDAS in the brain. These studies suggested that [ $^{11}\text{C}$ ]MeDAS-PET is a specific imaging marker of demyelination, but not neuroinflammation.

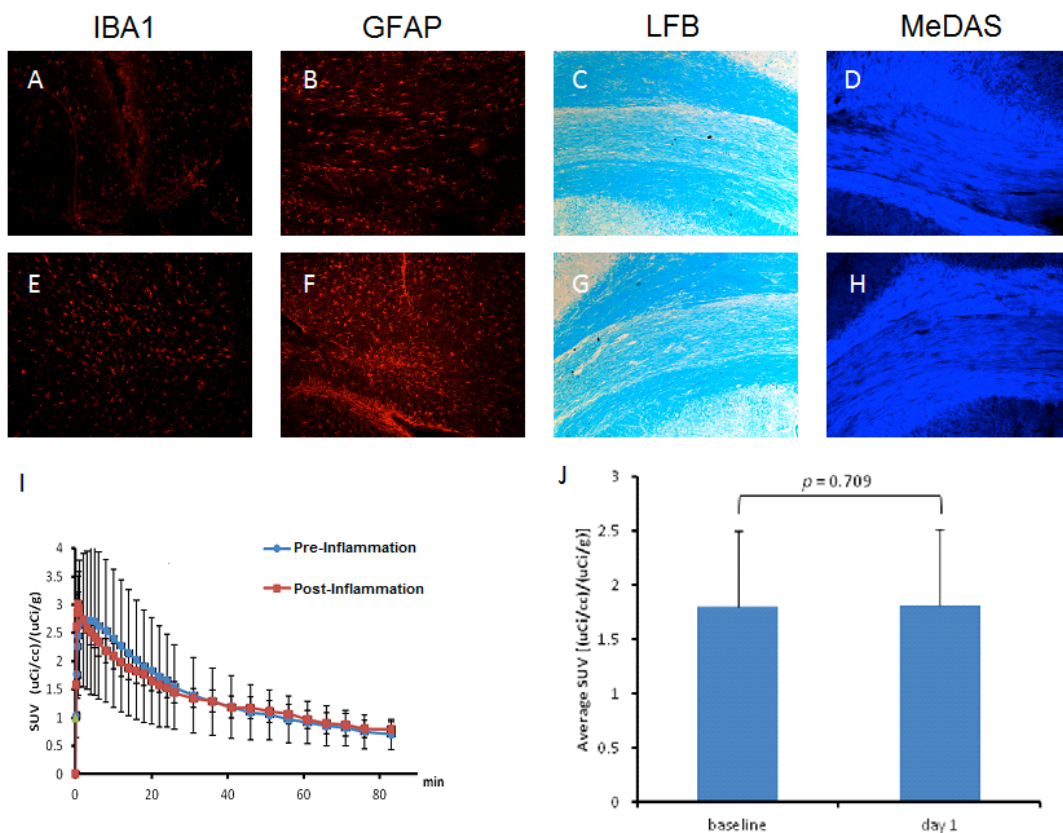


**Figure 4:** Immunohistochemical staining and [ $^{11}\text{C}$ ]MeDAS-PET studies in the rat brain at 24 hours after induction of neuroinflammation by LPS. A-D: Immunohistochemical staining of the right hemisphere of the rat brain including IBA1 staining of activated microglia and macrophages (A), GFAP staining of astrocytes in reactive form (B), Luxol Fast Blue and MeDAS staining of intact myelin tract (C and D). E-H: the corresponding staining results in the left hemisphere. I. [ $^{11}\text{C}$ ]MeDAS uptake as a function of time over the 90 min scan showing similar pharmacokinetic profiles before and after induction of inflammation. J. Average brain uptake of [ $^{11}\text{C}$ ]MeDAS over the 90 min of PET scan suggesting that neuroinflammation has no effects on [ $^{11}\text{C}$ ]MeDAS uptake.

### **Longitudinal PET imaging of the spinal cord in a LPC rat model**

We then evaluated the ability of [ $^{11}\text{C}$ ]MeDAS-PET to longitudinally assess myelin content in the spinal cord *in vivo*. To quantitatively characterize demyelination and remyelination, we first induced a focal demyelinated lesion (T11-12) by stereotactic injection of LPC to the spinal cord. The rat was then subjected to a serial PET/CT imaging at the peak of demyelination (7 days post injection), and during the course of remyelination (14 and 21 days post injection). As shown in **Figure 5A**, the rat spinal cord was readily visualized by [ $^{11}\text{C}$ ]MeDAS-PET with high specificity and sensitivity. The uptake of [ $^{11}\text{C}$ ]MeDAS in the affected region of the spinal cord at various time points was quantified. As shown in **Figure 5B**, [ $^{11}\text{C}$ ]MeDAS uptake was lowest at day 7 when demyelination was peaked. At day 14 and day 21 post injection, [ $^{11}\text{C}$ ]MeDAS uptake gradually increased due to anticipated remyelination.

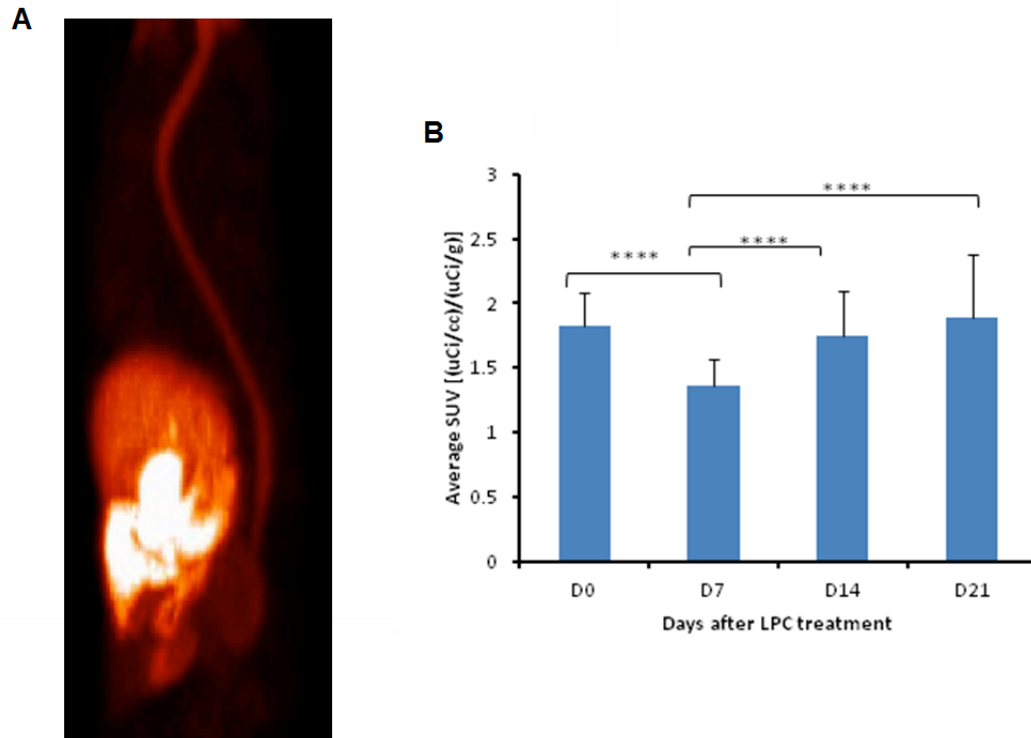


**Figure 5.** A: representative PET image of the rat spinal cord. B: Longitudinal PET studies in the LPC-treated rats over 21 days. The average uptake in the spinal cord (T11-T12) was quantified on day 0, 7, 14, and 21. On day 7 of demyelination, the uptake of [ $^{11}\text{C}$ ]MeDAS in the T11-T12 region decreased by 34% compared to day 0. On day 14 and 21 of remyelination, the uptake of [ $^{11}\text{C}$ ]MeDAS in the T11-T12 region increased by 22% and 28%, respectively, compared to day 7.

### Longitudinal PET imaging of the spinal cord in EAE rat model

While the LPC model represents pure demyelination/remyelination, EAE is the animal model that closely mimics the MS pathology. We thus conducted a series of [ $^{11}\text{C}$ ]MeDAS-PET imaging in an EAE rat model to longitudinally monitor myelination in the spinal cord. In this study, EAE was induced by immunizing 3 SD rats and 3 Lewis rats with MOG1-125 peptide. Starting at day 7 after immunization, the SD and Lewis rats developed paralysis of hind limbs, with an EAE score reaching 3.0 or above in a relapsing and remitting pattern. In this study, we conducted longitudinal PET imaging at three time remitting points of the disease. [ $^{11}\text{C}$ ]MeDAS

uptake in different vertebrae regions was quantified. In the EAE SD rats, [ $^{11}\text{C}$ ]MeDAS was not evenly distributed across the spinal cord. Before immunization, [ $^{11}\text{C}$ ]MeDAS uptake was relatively high in part of the thoracic region (T10-T13) (**Figure 6A**). After immunization, [ $^{11}\text{C}$ ]MeDAS uptake was significantly decreased across the whole spinal cord, particularly between T10-T13 in the thoracic region (**Figure 6B**). The average [ $^{11}\text{C}$ ]MeDAS uptake was determined from L3 to T8 at the three episodes on days 15, 25, and 42 (**Figure 6C**). Compared to pre-immunization, the average [ $^{11}\text{C}$ ]MeDAS uptake decreased significantly at all three episodes (**Figure 6C**). Particularly at the third episode on day 42 when the EAE score was almost 5.0, [ $^{11}\text{C}$ ]MeDAS uptake reached the lowest level (**Figure 6D**). The greatest change was observed in the region between T10-T13 as shown in the representative PET and CT fusion image of the spinal cord in the SD rat on day 42 after immunization with MOG1-125, which was reconstructed based on uptake of [ $^{11}\text{C}$ ]MeDAS (**Figure 7**).

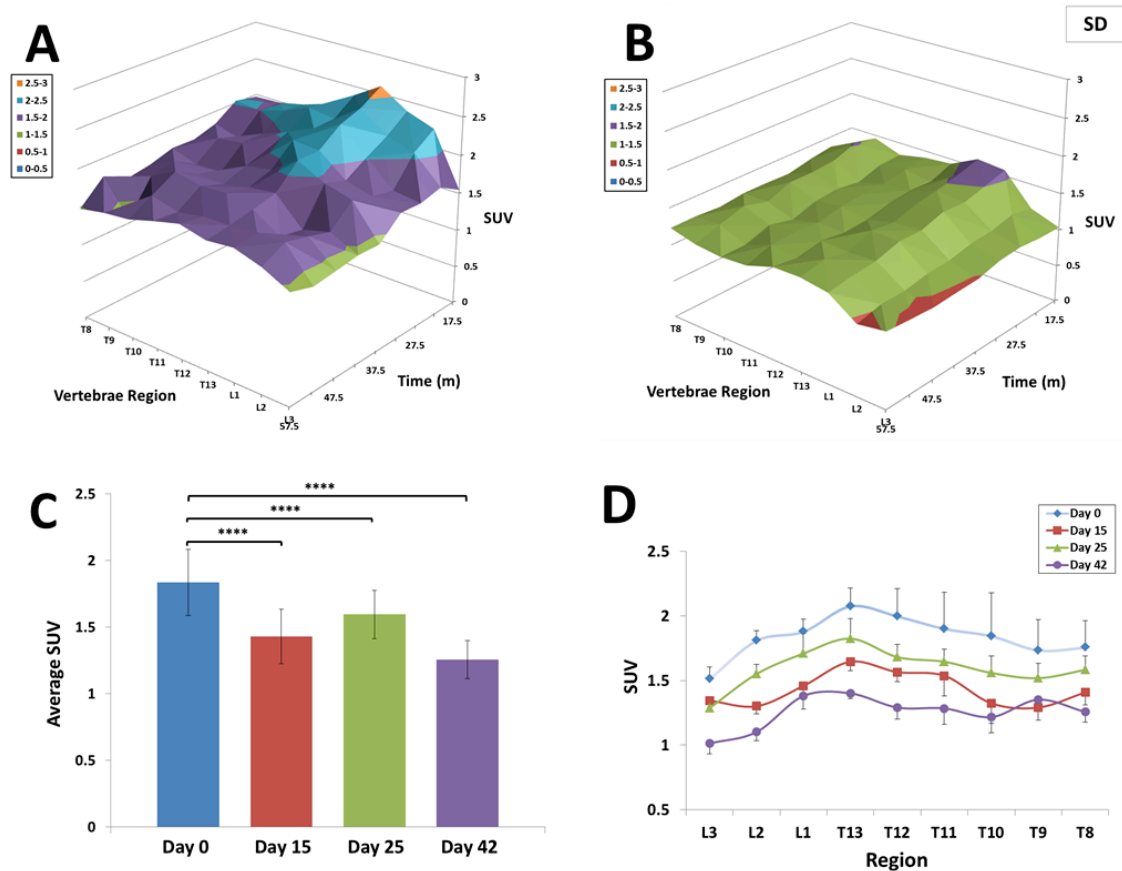


**Figure 6.** A:  $[^{11}\text{C}]\text{MeDAS}$  uptake across regions L3-T8 from 17.5 min to 57.5 min of a control SD rat. B:  $[^{11}\text{C}]\text{MeDAS}$  uptake across regions L3-T8 from 17.5 min to 57.5 min of an EAE SD rat after immunization with MOG1-125. Note homogenized demyelination in these regions, characterized by a lower SUV. C: Average SUV values over the L3-T8 region in the SD rat on day 0, 15, 25, and 42. D: Average SUV values by spinal region in SD rat for each scan. Note the most prominent changes occur in the L3-T8 region. Error bars refer to absolute error.

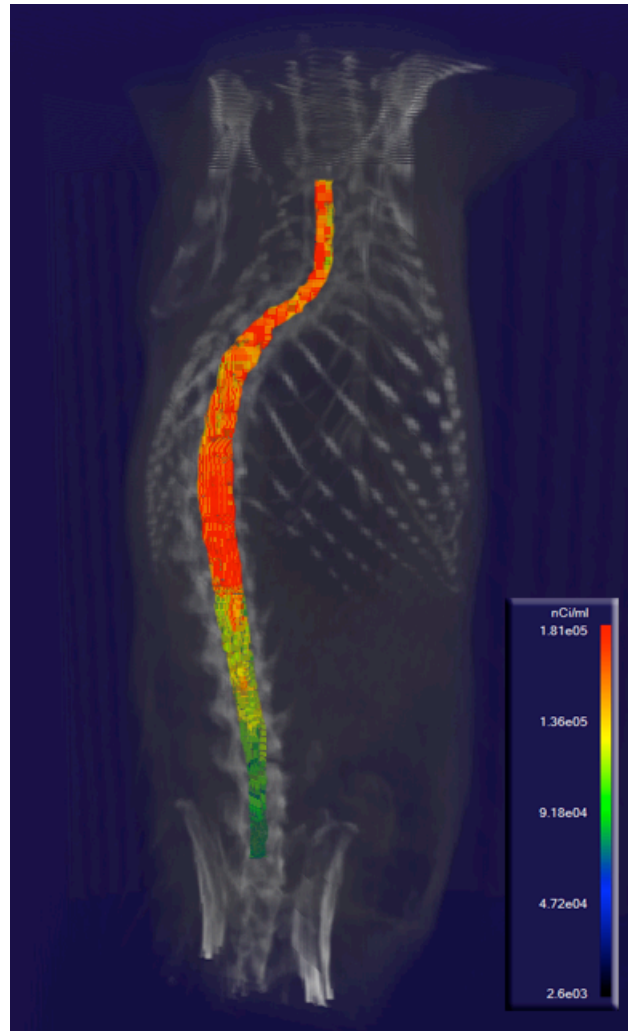


**Figure 7.** Three-dimensional PET and CT fusion image of the spinal cord in a SD rat on day 42 after immunization with MOG1-125.

In the EAE Lewis rats, similar pattern of [ $^{11}\text{C}$ ]MeDAS distribution was observed. Before immunization, [ $^{11}\text{C}$ ]MeDAS uptake was relatively high in the thoracic region between T9-T13 (**Figure 8A**). After immunization, [ $^{11}\text{C}$ ]MeDAS uptake decreased significantly in the lumbar regions (L1-L6) compared to other regions in the spinal cord (**Figure 8B**). The average [ $^{11}\text{C}$ ]MeDAS uptake was then determined at the three peaks of the disease: on days 26, 33,

and 39 (**Figure 8C**). This is particularly apparent at the third episode when the EAE symptom was most severe. Unlike the EAE SD rats, the EAE Lewis rats showed the most difference in the lumbar region between L1 and L6 (**Figure 8D**). Post-mortem histochemical staining using both MeDAS and Black-Gold displayed significantly low fluorescence in the white matter of the spinal cord (**Figure 2E and 2F**).

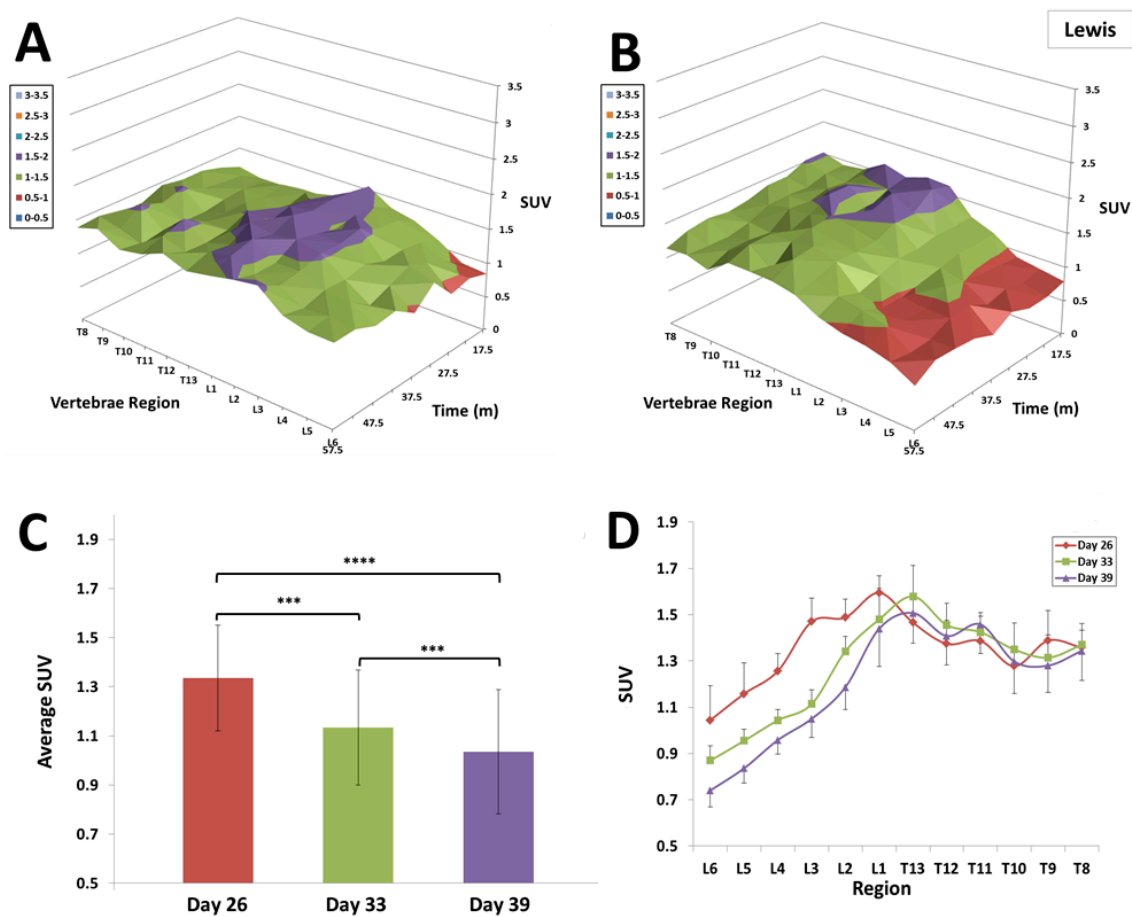


**Figure 8.** A:  $[^{11}\text{C}]\text{MeDAS}$  uptake across regions L6-T8 from 17.5 min to 57.5 min of a control Lewis rat. B:  $[^{11}\text{C}]\text{MeDAS}$  uptake across regions L6-T8 from 17.5m to 57.5m of an EAE Lewis rat. Note significant demyelination in the Lumbar vertebrae, characterized by a lower SUV in these areas. C: Average SUV values over the L6-L1 region in the EAE Lewis rat on day 26, 33, and 39 after



immunization of MOG1-125. D: Average SUV values in the L6-T8 region in the EAE Lewis rat for each scan. Note there is significant differentiation only in the Lumbar. Error bars refer to absolute error.

### **Limit to detect demyelination and remyelination**

The limit to detect demyelination and remyelination by [<sup>11</sup>C]MeDAS-PET is determined by multiple factors, including the detection efficiency of PET scanner, specific activity of radioligands, and binding affinity for myelin. Our previous study showed that binding affinity (K<sub>d</sub>) of such type of myelin-imaging agents was in the range of 1 nM with a B<sub>max</sub> of 17pmol/mg (Wang et al., 2009). The detection efficiency of newly calibrated PET scanner (Inveon PET/CT, Siemens) is 2479.188 nCi per voxel. The specific activity of [<sup>11</sup>C]MeDAS was determined as 3 Ci/mmol, or 826.4 pmol of [<sup>11</sup>C]MeDAS per voxel. According to biodistribution studies (Table 1), MeDAS brain uptake is averaged at 0.3 % at steady state, this correlates to a detection limit of 0.71mg myelin change per voxel, as estimated by:

$$\text{detection limit} = \frac{(B_{\max})}{(K_d)} \times \frac{(\text{detection efficiency})}{(\text{specific activity})} \times (\text{brain uptake}) \times (\text{molecular weight})$$

### **Image-guided myelin repair therapy**

Based on the longitudinal studies, we conducted the first image-guided myelin repair therapy in a rat model of focal demyelination to monitor myelin changes in the spinal cord and determine the dose response of HGF, a multifunctional growth factor that has been proven to be the effective component in MSC therapy of myelin repair (Bai et al., 2012). In this study, rats were first treated with LPC to induce demyelination in the spinal cord. On days 7 and 9, the rats were sequentially treated with HGF, and imaged by [<sup>11</sup>C]MeDAS-PET on days 7, 14, and 21. At a dose of 100 ng/rat or 0.4 µg/kg, the HGF-treated rats displayed an increased [<sup>11</sup>C]MeDAS uptake in the spinal cord compared to the control rats. Quantitative analysis showed the HGF

treatment caused the average uptake in the demyelinated regions to be 31% and 14% greater at day 14 and 21 respectively, when compared with day 7 (**Figure 9**). When the rats were treated with a higher dose of HGF (i.e. 200 ng/rat or 0.8 ug/kg), the maximal remyelinating effect was observed to be 33% and 35% on days 14 and 21, respectively. Note there is only a significant difference in the amount of remyelination on day 21, on day 14, the difference in remyelination provided by the additional dose of HGF is not significant. The imaging results were confirmed by double-blinded immunohistochemical observations of postmortem tissue sections harvested at each time point (Bai et al., 2012).

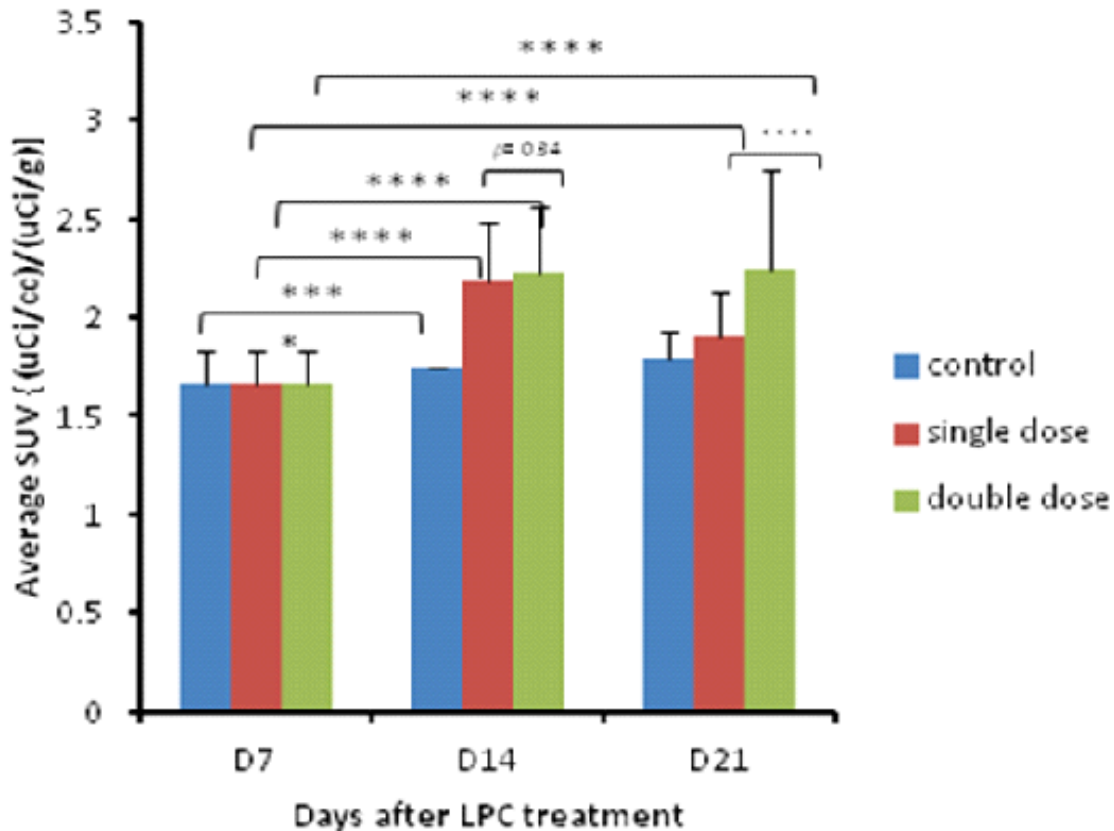


**Figure 9.** Longitudinal quantitative PET analysis of myelin changes in the spinal cord (T11-12) of a LPC-treated rat model on Day 7, 14, and 21 following HGF-treatment. Increased specific uptake of [ $^{11}\text{C}$ ]MeDAS in spinal cords of HGF treated versus control. Following HGF treatment at a dose of 100

ng/rat or 0.4 ug/kg, the average uptake of [ $^{11}\text{C}$ ]MeDAS increased by 31% and 14% compared to the control on day 14 and 21, respectively. When the HGF dose were doubled, the average uptake of [ $^{11}\text{C}$ ]MeDAS increased by 33% and 35% compared to the control on day 14 and 21, respectively.

### **Rodent-based dosimetry estimates of [ $^{11}\text{C}$ ]MeDAS**

In order to conduct future characterization of [ $^{11}\text{C}$ ]MeDAS in humans, rodent-based dosimetry of [ $^{11}\text{C}$ ]MeDAS was estimated. The single organ and whole body radiation exposure associated with [ $^{11}\text{C}$ ]MeDAS injection was determined from the biodistribution data obtained in mice. Based on the biodistribution, dosimetry was estimated using OLINDA/EXM(Stabin et al., 2005) software. Based on an extrapolation of the animal data to humans, the radiation doses estimated for various human organs are summarized in **Table 2**.

**Table 2.** Organ and whole body extrapolated human dosimetry estimation.

<u>Target Organ</u>	<u>mSv/MBq</u>	<u>rem/mCi</u>
Adrenals	4.31E-03	1.59E-02
Brain	1.89E-03	7.01E-03
Breasts	2.25E-03	8.34E-03
Gallbladder Wall	3.28E-03	1.21E-02
LLI Wall	3.03E-03	1.12E-02
Small Intestine	3.10E-03	1.15E-02
Stomach Wall	2.93E-03	1.08E-02
ULI Wall	3.06E-03	1.13E-02
Heart Wall	2.30E-03	8.49E-03
Kidneys	2.72E-03	1.00E-02
Liver	4.64E-03	1.72E-02
Lungs	2.91E-03	1.08E-02
Muscle	2.60E-03	9.61E-03
Ovaries	3.12E-03	1.15E-02
Pancreas	3.15E-03	1.16E-02
Red Marrow	3.62E-03	1.34E-02
Osteogenic Cells	6.76E-03	2.50E-02
Skin	2.14E-03	7.92E-03
Spleen	2.41E-03	8.94E-03
Testes	2.58E-03	9.53E-03
Thymus	2.69E-03	9.94E-03
Thyroid	2.69E-03	9.94E-03
Urinary Bladder Wall	2.99E-03	1.11E-02
Uterus	3.14E-03	1.16E-02
Total Body	2.85E-03	1.05E-02
Effective Dose Equivalent	3.30E-03	1.22E-02
Effective Dose	2.99E-03	1.10E-02

### Acute Toxicity study

Following dosimetry estimation, we also evaluated the acute toxicity in mice. A total of 30 mice were divided into 5 groups, which were injected with escalating doses ranging from 82 mg/kg to 168 mg/kg. Based on the survival percentage, we calculated the LD<sub>50</sub> of MeDAS as 141 mg/kg, which is well in the safety margin, as it is in the 6 orders of magnitude higher than the amount needed for the *in vivo* PET imaging studies.

## DISCUSSION

Current therapeutic strategies primarily target the immunopathological basis of demyelination.

The outcome from this approach has not been particularly successful, as most therapies

continue to be directed toward widespread immuno-suppression, and do little to promote long lasting repair. As such, they are of limited value for supporting long-term functional restoration. For long term functional recovery in patients with MS and related acquired demyelinating diseases, tremendous efforts have been made to utilize the information generated from pathobiological studies on the development of myelinating oligodendrocyte cells of the CNS, to the identification of targets and characterization of new therapeutic approaches towards promoting lasting remyelination in the adult CNS.

For drug discovery and development in myelin repair therapy, one major challenge has been assessing and quantifying changes in myelin content *in vivo*. To date, magnetic resonance imaging (MRI) has been the primary tool for diagnosing and monitoring the demyelinating conditions in MS. Unfortunately, any change in signal intensity on a dual echo T2-weighted sequence reflects a change in tissue water content, which is a non-specific measure of the overall changes in macroscopic tissue injury and ranges from edema and inflammation, to demyelination and axonal loss. As a result, MRI changes do not specifically reflect changes in demyelination and remyelination. It is thus essential to develop a measure that will effectively correlate clinical outcomes directly with myelin content. For this reason, we propose to detect and quantify myelin changes based on PET. PET imaging is a noninvasive imaging technique capable of direct characterization and quantification of biological processes at the molecular level (Phelps, 2000). It has become one of the most important clinical techniques in the diagnosis, prognosis, and monitoring of disease progression. This powerful imaging technique is used in conjunction with trace amounts of positron-emitting radiotracers that are specific for targets of interest.

For *in vivo* detection and quantification of myelin changes, radiotracers must readily enter the brain and specifically bind to myelin sheaths. To date, lack of myelin-specific imaging radiotracers has hampered the application of PET in monitoring demyelination and remyelination. As a result, PET study in MS is limited to the characterization of neuroinflammation using [ $^{18}\text{F}$ ]FDG for glucose metabolism or [ $^{11}\text{C}$ ]PK11195 for peripheral benzodiazepine receptors (PBR) mediated microglia activation (Cuzner, 1997; Wilms et al., 2003; Chen and Guilarte, 2006; Buck et al., 2012). However, such radiotracers are not specific for the characterization of demyelination and remyelination, so they do not provide any correlation of disease progression in MS. Most recently, a F-18 labeled mitochondrial 18kDa translocator protein (TSPO) radioligand termed [ $^{18}\text{F}$ ]DPA-714, has also been developed to image microglial/macrophage activation present in the experimental autoimmune encephalomyelitis (EAE) rat model (Abourbeh et al., 2012). Similar to PBR, TSPO only mediates neuroinflammation (Winkeler et al.; Banati, 2002; Dolle et al., 2009). Thus, [ $^{18}\text{F}$ ]DPA-714 PET can only be used for imaging inflammation, not myelination.

A new strategy is to develop therapeutic agents that are aimed at stimulating remyelination in damaged neural tissues. To date, the development of such myelin repair therapeutics for MS has been hampered by the lack of imaging approaches that allow for direct detection and quantification of myelin changes in a longitudinal manner. In order to meet this challenge, we developed a series of radiotracers for PET imaging of myelination. To identify the most promising PET imaging markers for downstream clinical studies, we used the following set of quantitative acceptance criteria to guide our evaluation processes: 1) High brain uptake at early time points following i.v. injection. At 5 min post injection, the brain concentration of probe should reach 5% ID/g; 2) Average retention in white matter should be at least 20% higher than that in the adjacent gray matter in the spinal cord; 3) In animal models of MS,

radioactivity concentration in demyelinated regions should be significantly lower than that in non-demyelinated regions, based on the same size of regions of interest; 4) Radioactive metabolites in plasma should be hydrophilic, and not permeable across the BBB to avoid diluting the specific uptake signal; 5) Rapid clearance of radiotracer from other organs (e.g., lung, heart, liver, etc) to ensure optimal dosimetry; 6) Minimal probe toxicity with an LD<sub>50</sub> ≥10 mg/kg, or 1,000 times higher than the amount to be injected in future human subjects to ensure a wide margin of safety.

Accordingly, [<sup>11</sup>C]MeDAS exhibits a promising profile of *in vivo* binding properties and toxicity. Biodistribution studies showed that it readily entered the brain at early time points with 6.07 ID/g at 5 min. After entering the brain, [<sup>11</sup>C]MeDAS was proportionally localized in the white matter vs. gray matter. In the brain, the average retention in the white matter is ca. 40% higher than in the gray matter (**Figure 3A**). In demyelinated regions, the uptake of [<sup>11</sup>C]MeDAS was significantly decreased. In the model of focal demyelination introduced by LPC, for example, [<sup>11</sup>C]MeDAS uptake was 34% lower in the demyelinated regions compared to intact myelinated regions in the spinal cord. Further studies showed that the radioactive metabolites of [<sup>11</sup>C]MeDAS are hydrophilic and expected not to be permeable across the BBB to interfere with the specific uptake signal. Based on the biodistribution studies, the dosimetry of [<sup>11</sup>C]MeDAS was estimated, and these data sets were all well fit with single exponential functions. Most organs appear to receive around 0.002-0.005 mGy/MBq. The total exposure resulting from a 10 mCi administration of [<sup>11</sup>C]MeDAS is far below the FDA-defined limits for yearly cumulative and per study exposures to research participants, and is comparable with other radiotracers widely used in the clinic. Acute toxicity studies also showed that [<sup>11</sup>C]MeDAS was safe for potential human studies, with a LD<sub>50</sub> of 141 mg/Kg or 6 order of magnitude higher than the actual dose needed for PET imaging studies in humans.

## **CONCLUSION**

The studies described above represent a unique imaging-guided approach to monitor disease and repair processes in demyelinating conditions in the CNS, with the absence of invasive surgeries or biopsies. The major advance in being able to utilize our newly developed myelin-imaging technique to quantify local levels of myelination, will for the first time, allow the development of therapeutics that are directly focused at recovery of lost neural tissue. Because myelin repair is critical for sustained functional recovery, the ability to directly track myelin levels in defined regions of the human CNS will allow us to assess the efficacy of new therapeutics in promoting myelin repair. Thus, the threshold for developing new MS therapeutics will be significantly reduced, and this application holds the promise of allowing new therapeutic development to proceed in a highly accelerated manner. As a consequence, the impact on MS patients will be profound as this novel approach could potentially revolutionize therapeutic development for demyelinating diseases, and hasten their widespread clinical application.



## REFERENCES

- Abourbeh G, Theze B, Maroy R, Dubois A, Brulon V, Fontyn Y, Dolle F, Tavitian B, Boisgard R (2012) Imaging microglial/macrophage activation in spinal cords of experimental autoimmune encephalomyelitis rats by positron emission tomography using the mitochondrial 18 kDa translocator protein radioligand [(1)(8)F]DPA-714. *J Neurosci* 32:5728-5736.
- Bai L, Lennon DP, Caplan AI, DeChant A, Hecker J, Kranso J, Zaremba A, Miller RH (2012) Hepatocyte growth factor mediates mesenchymal stem cell-induced recovery in multiple sclerosis models. *Nat Neurosci* 15:862-870.
- Banati RB (2002) Visualising microglial activation in vivo. *Glia* 40:206-217.
- Bot JC, Barkhof F, Polman CH, Lycklama a Nijeholt GJ, de Groot V, Bergers E, Ader HJ, Castelijns JA (2004) Spinal cord abnormalities in recently diagnosed MS patients: added value of spinal MRI examination. *Neurology* 62:226-233.
- Buck D, Forschler A, Lapa C, Schuster T, Vollmar P, Korn T, Nessler S, Stadelmann C, Drzezga A, Buck AK, Wester HJ, Zimmer C, Krause BJ, Hemmer B (2012) 18F-FDG PET detects inflammatory infiltrates in spinal cord experimental autoimmune encephalomyelitis lesions. *J Nucl Med* 53:1269-1276.
- Chen MK, Guilarte TR (2006) Imaging the peripheral benzodiazepine receptor response in central nervous system demyelination and remyelination. *Toxicol Sci* 91:532-539.
- Ciccarelli O, Wheeler-Kingshott CA, McLean MA, Cercignani M, Wimpey K, Miller DH, Thompson AJ (2007) Spinal cord spectroscopy and diffusion-based tractography to assess acute disability in multiple sclerosis. *Brain* 130:2220-2231.
- Cuzner ML (1997) Microglia in health and disease. *Biochem Soc Trans* 25:671-673.

- Dolle F, Luus C, Reynolds A, Kassiou M (2009) Radiolabelled molecules for imaging the translocator protein (18 kDa) using positron emission tomography. *Curr Med Chem* 16:2899-2923.
- Kerstetter AE, Padovani-Claudio DA, Bai L, Miller RH (2009) Inhibition of CXCR2 signaling promotes recovery in models of multiple sclerosis. *Exp Neurol* 220:44-56.
- Mi S, Hu B, Hahm K, Luo Y, Kam Hui ES, Yuan Q, Wong WM, Wang L, Su H, Chu TH, Guo J, Zhang W, So KF, Pepinsky B, Shao Z, Graff C, Garber E, Jung V, Wu EX, Wu W (2007) LINGO-1 antagonist promotes spinal cord remyelination and axonal integrity in MOG-induced experimental autoimmune encephalomyelitis. *Nat Med* 13:1228-1233.
- Phelps ME (2000) Positron emission tomography provides molecular imaging of biological processes. *Proc Natl Acad Sci U S A* 97:9226-9233.
- Stabin MG, Sparks RB, Crowe E (2005) OLINDA/EXM: the second-generation personal computer software for internal dose assessment in nuclear medicine. *J Nucl Med* 46:1023-1027.
- Stankoff B, Wang Y, Bottlaender M, Aigrot MS, Dolle F, Wu C, Feinstein D, Huang GF, Semah F, Mathis CA, Klunk W, Gould RM, Lubetzki C, Zalc B (2006) Imaging of CNS myelin by positron-emission tomography. *Proc Natl Acad Sci U S A* 103:9304-9309.
- Wang C, Wu C, Zhu J, Miller RH, Wang Y (2010a) Design, synthesis, and evaluation of coumarin-based molecular probes for imaging of myelination. *J Med Chem* 54:2331-2340.
- Wang C, Popescu DC, Wu C, Zhu J, Macklin W, Wang Y (2010b) In situ fluorescence imaging of myelination. *J Histochem Cytochem* 58:611-621.
- Wang C, Wu C, Popescu DC, Zhu J, Macklin WB, Miller RH, Wang Y (2011) Longitudinal near-infrared imaging of myelination. *J Neurosci* 31:2382-2390.

- Wang Y, Wu C, Caprariello AV, Somoza E, Zhu W, Wang C, Miller RH (2009) In vivo quantification of myelin changes in the vertebrate nervous system. *J Neurosci* 29:14663-14669.
- Wenk GL, McGann-Gramling K, Hauss-Wegrzyniak B, Ronchetti D, Maucci R, Rosi S, Gasparini L, Ongini E (2004) Attenuation of chronic neuroinflammation by a nitric oxide-releasing derivative of the antioxidant ferulic acid. *J Neurochem* 89:484-493.
- Wilms H, Claasen J, Rohl C, Sievers J, Deuschl G, Lucius R (2003) Involvement of benzodiazepine receptors in neuroinflammatory and neurodegenerative diseases: evidence from activated microglial cells in vitro. *Neurobiol Dis* 14:417-424.
- Winkeler A, Boisgard R, Martin A, Tavittian B Radioisotopic imaging of neuroinflammation. *J Nucl Med* 51:1-4.
- Wu C, Wei J, Tian D, Feng Y, Miller RH, Wang Y (2008) Molecular probes for imaging myelinated white matter in CNS. *J Med Chem* 51:6682-6688.
- Wu C, Wang C, Popescu DC, Zhu W, Somoza EA, Zhu J, Condie AG, Flask CA, Miller RH, Macklin W, Wang Y (2010) A novel PET marker for in vivo quantification of myelination. *Bioorg Med Chem* 18:8592-8599.
- Wu C, Tian D, Feng Y, Polak P, Wei J, Sharp A, Stankoff B, Lubetzki C, Zalc B, Mufson EJ, Gould RM, Feinstein DL, Wang Y (2006) A novel fluorescent probe that is brain permeable and selectively binds to myelin. *J Histochem Cytochem* 54:997-1004.